ACS OMEGA

Open Access

http://pubs.acs.org/journal/acsodf

Article

Dissociative Photoionization of Dimethylpyridines and Trimethylpyridine at 266 nm: Dynamics of Methyl Radical Release

Sumitra Singh, Monali Kawade, and G. Naresh Patwari*

Cite This: *ACS Omega* 2024, 9, 8173−8178

Read Online

ACCESS | Metrics & More | Article Recommendations | Supporting Information

ABSTRACT: The 266 nm photolysis of various positional isomers of dimethylpyridines and trimethylpyridine was investigated by measuring the translational energy distribution of the methyl radical following $\{sp^2\}C-C\{sp^3\}$ bond dissociation. The observed translational energy distribution is attributed to the dissociative photoionization in the cationic ground state following [1 + 1 + 1] three-photon absorption. The translational energy distribution profiles of the methyl radical were broad with the maximum translation energy in excess of 2 eV, which originates due to the dissociation of $\{sp^2\}C-C\{sp^3\}$ bond ortho to the N atom in the ring. The dynamics of $\{sp^2\}C-C\{sp^3\}$ bond dissociation in the cationic ground state of methylpyridines is marginally dependent on the number and position of the methyl groups; similar to xylenes, however, it is site-selective with the preferential cleavage of C−C bond in the ortho position to the pyridinic nitrogen atom, which is attributed to the relative stability of the resulting radical cation.

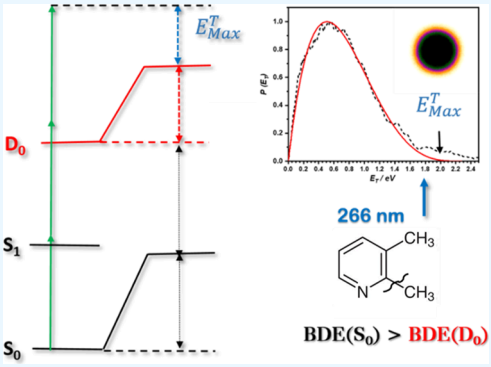

INTRODUCTION

Understanding the photodissociation dynamics of aromatic molecules is crucial in the exploration of photophysical properties of complex biomolecules, wherein methylated aromatic compounds are fundamental building blocks for complex biomolecules.[1−5] Among various aromatic molecules, the heterocyclic analogs are important due to their hierarchy in natural selection in the composition of complex biomolecular systems and the heterocyclic analogs of methylated aromatic compounds in particular, such as nucleobase uracil. Changes in the electronic structure and symmetry of the electronic states depending on the type and position of heteroatom substitution within an aromatic ring are known to influence the photophysical properties of these molecules.[6−11] In the case of benzene, the absorption of a single photon within the 190−270 nm range gives rise to various radiative and nonradiative decay processes, such as isomerization, photodissociation involving H atom elimination, and ring opening.[1,4,12] On the other hand, the photodissociation dynamics of N-substituted heterocyclic analogs of benzene, *viz.*, pyridine and pyrimidine, exhibit a reduction in the threshold for ring-opening reactions as the number of nitrogen atoms in the ring increases.[13] Nevertheless, the alkyl-substituted derivatives of both the systems, namely, methylbenzenes and methylpyridines, undergo extensive isomerization following excitation to the excited singlet electronic states, resulting in various positional isomers due to the scrambling of the alkyl substituent.[2,14−19] Subsequent to internal conversion to the ground electronic state, the $\{sp^2\}C-C\{sp^3\}$ and C−H bond fission are the major photodissociation channels in these molecules.[20−24] Furthermore, isomerization from being a six-membered to seven-membered via a C−C bond insertion mechanism has also been reported.[2,25,26] Interestingly, the energy barrier associated with the insertion-isomerization process (about 4.60 eV)[19,27,28] is comparable to the $\{sp^2\}C-C\{sp^3\}$ bond dissociation threshold (around 4.50 eV),[29] thereby resulting in a compelling interplay of competing pathways. Furthermore, the presence of an aromatic chromophore enhances the likelihood of (resonant) multiphoton absorption, allowing the molecules to access both the ground and excited states of the cation.[30−32] In the case of xylenes and mesitylene, 266 nm excitation leads to dissociative photoionization resulting in $\{sp^2\}C-C\{sp^3\}$ bond fission and formation of a methyl radical via a resonant three-photon absorption process, which is attributed to the substantial lowering of the $\{sp^2\}C-C\{sp^3\}$ bond dissociation energy in the cation ground state relative to the neutral ground state.[33] In light of these observations, photodissociation studies on methylpyridines following 266 nm excitation were carried out on N-heterocyclic analogues of xylene and mesitylene using the velocity map ion imaging (VMI) technique. Comparison of the dissociative photoionization process in xylene and mesitylene with the corresponding pyridine analogs provides insights into the role of electronic

Received: November 2, 2023
Revised: December 22, 2023
Accepted: January 23, 2024
Published: February 8, 2024

https://doi.org/10.1021/acsomega.3c08705
ACS Omega 2024, 9, 8173−8178

effects due to heteroatom substitution on the $\{sp^2\}C-C\{sp^3\}$ bond dissociation. Figure 1 depicts the molecular structures of

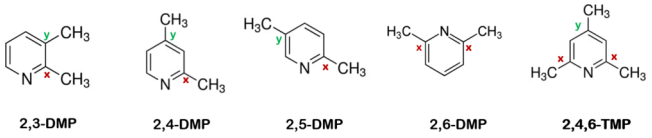

Figure 1. Structures of the positional isomers of DMPs and TMP. The indices *x* and *y* denote the types of methyl groups present in each molecule, depending on their respective positions relative to the nitrogen atom.

various positional isomers of dimethylpyridines (DMPs) and trimethylpyridine (TMP) considered in the present work. Unlike methylbenzenes, the methyl groups present in methylpyridines exhibit variations based on their proximity to the nitrogen atom, which are denoted as *x* and *y* labels for methyl groups located closer and farther from pyridine nitrogen, respectively, with the exception of symmetric 2,6-dimethylpyridine. A pertinent question that arises is whether dissociation of one the $\{sp^2\}C-C\{sp^3\}$ bond is preferred over the other.

METHODOLOGY

The experimental setup for carrying out velocity map imaging experiments is described elsewhere.[34] Succinctly, a skimmed molecular beam of reagent-doped helium buffer gas (3 atm) was intersected by a counter-propagating pump (266 nm) and probe (333.45 nm) lasers, and the resulting cations were then captured and imaged using a four-electrode VMI spectrometer equipped with a 50 mm diameter two-stage microchannel plate (MCP) and a P47 phosphor screen (MCP-50DLP47VF; Tectra). The image on the phosphor screen was captured using a high-performance, easy-to-use USB, GigE CMOS camera (IDS Imaging Development Systems), and the image was acquired using NuAcq software.[35] All the images were acquired for about 50,000 laser shots and were further processed (symmetrized) using ImageJ software,[36] and Abel inversion was carried out by the basis set expansion method to extract the translational energy spectrum.[37] In the present set of experiments, the pump laser (266 nm) is generated as the fourth harmonic of a Nd:YAG laser (Brilliant-B; Quantel), while the probe laser (333.45 nm) is produced by frequency-doubling the output of a tunable dye laser (LiopStar-HQ; LIOP-TEK), which is pumped with the second harmonic of a Nd:YAG laser (Brilliant-B; Quantel). The polarization planes of both lasers were aligned parallel to the detector plane. The time delay between the pump and probe lasers was approximately 10 ns. The time delays between various operational elements, such as the opening of the pulsed nozzle, triggering of both flashlamp and Q-switch for laser firing, gating of the front-plate of the MCP detector, and opening of the camera shutter, were controlled by an eight-channel digital delay pulse generator (DDG-9520; Quantum Composers). The pump and probe lasers were operated at energies of approximately 500 and 200 μJ/pulse, respectively, and were focused onto the molecular beam using a plano-convex lens with a focal length of 350 mm. The pump beam had a spot size (around 1 mm) that was slightly larger than that of the probe beam (less than 1 mm). The laser flux was carefully adjusted to ensure that the signal intensity from the methyl fragment was negligible in the absence of a probe laser.

RESULTS AND DISCUSSION

The mass spectra obtained following 266 nm photolysis of the various positional isomers of DMP and TMP are presented in Figure S1 (see the Supporting Information). The mass spectra, in all the cases, show intense peaks corresponding to the molecular ion at m/z = 107 $[C_5H_3N(CH_3)_2]^+$ and m/z = 121 $[C_5H_2N(CH_3)_3]^+$ for DMPs and TMP, respectively, along with several weaker peaks corresponding to C_nH_m (n = 2−6), fragments of which were observed in all cases. The pump−probe mass spectra additionally exhibit a peak corresponding to the methyl radical at m/z = 15, which was probed using a 333.45 nm laser with [2 + 1] REMPI following excitation to the Q-branch of the 0_0^0 band of the $X\sim^2A_2'' \rightarrow 3p^2A_2''$ transition.[38,39] Furthermore, the pump−probe mass spectra also reveal an increase in the intensity of peaks corresponding to molecular fragments of C_nH_m (where n = 2, 3), suggesting the extensive probe-induced fragmentation of the parent molecule leading to the production of smaller fragments. The velocity map images of the methyl fragments and the corresponding total translational energy release distribution profiles $[P(E_T)]$ are depicted in Figure 2. The velocity map images of methyl fragments are isotropic and diffused in nature, characterized by a central blob-like feature, indicating a broader translational energy distribution.[34] This isotropic nature suggests that the scission of the $\{sp^2\}C-C\{sp^3\}$ bond follows a predissociation pathway with a longer time scale compared to the rotational reorientation times, in contrast to the case of methyl iodide or dimethyl sulfide.[40,41] For a quantitative understanding of the trends observed in total translational energy release distributions obtained from experiments, the-$\{sp^2\}C-C\{sp^3\}$ bond dissociation energies (BDE) of the molecules under investigation were calculated in their neutral $[BDE(S_0)]$ and cationic $[BDE(D_0)]$ ground states with the G3B3[42] method using Gaussian-09.[43] Table 1 lists the values of the calculated BDE along with the calculated ionization energies and $S_0 \rightarrow S_1$ vertical transition energies (calculated using CAM-B3LYP/6-311G(d,p)) for all the molecules.

A generalized energy-level scheme for the formation of methyl radicals, shown in Figure 3, considers the $\{sp^2\}C-C\{sp^3\}$ BDE in both the neutral and cationic ground states. In all cases, the calculated $\{sp^2\}C-C\{sp^3\}$ bond dissociation energy in the neutral ground state $[BDE(S_0)]$ (see Table 1) is approximately 0.3 eV lower than the photon energy of 266 nm (4.66 eV). Consequently, the $\{sp^2\}C-C\{sp^3\}$ bond dissociation in the S_0 state would result in a maximum total translational energy E_T^{max} of about 0.3 eV, which is much lower than the experimentally observed value (see Figure 2) and rules out the possibility of formation of the methyl radical dissociation from the neutral ground state. Furthermore, the $S_0 \rightarrow S_1$ transition energy is marginally less than 4.66 eV for all cases (see Table 1), which suggests that the absorption of the first 266 nm photon leads to the vibronic excitation just above the band-origin 0_0^0 of the S_1 state. This excitation serves as a resonant intermediate level for the subsequent absorption of the second 266 nm photon, which results in the ionization of the molecules. The ionized molecules undergo $\{sp^2\}C-C\{sp^3\}$ bond dissociation in the cationic ground state $[BDE(D_0)]$ upon the absorption of the third photon. The calculated $[E_T^{max}]$ values using eq 1 based on this three-photon bond dissociation energy scheme are listed in Table 1 and can be observed in good agreement with the experimental total translational energy distribution profile $P(E_T)$ (Figure 2)

$$[E_T^{max}] = 3 \times 4.66 - IE - BDE(D_0) \text{in eV} \quad (1)$$

https://doi.org/10.1021/acsomega.3c08705
ACS Omega 2024, 9, 8173−8178

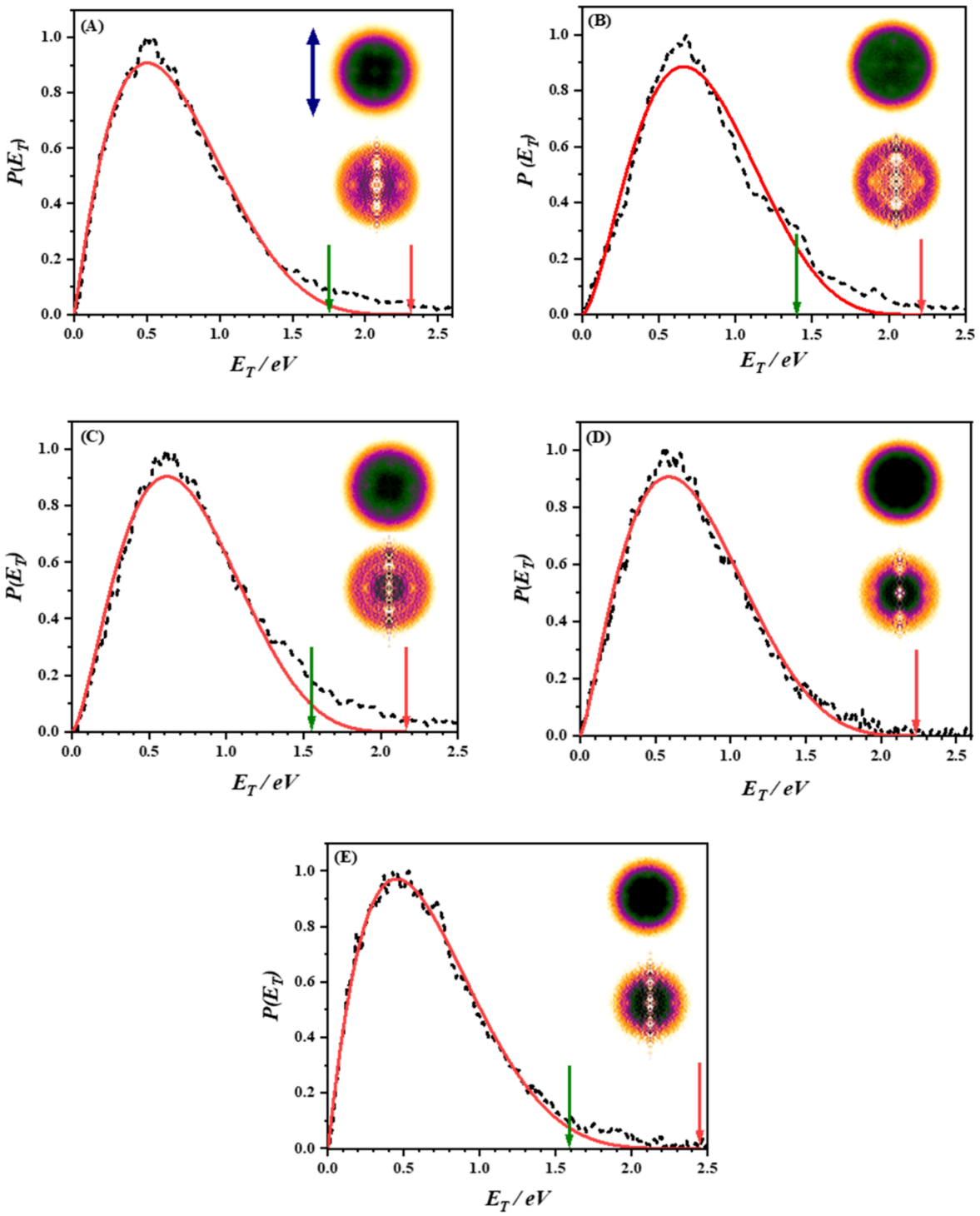

Figure 2. Total translational energy release distribution profiles $P(E_T)$ (black dashed traces) and their fits to eq 2 based on E_T^{max} values calculated for the $\{sp^2\}C-C\{sp^3\}$ bond marked "*x*" in Figure 1 (solid red curves) for (A) 2,3-DMP (a = 1.10; b = 4.0), (B) 2,4-DMP (a = 1.71; b = 4.0), (C) 2,5-DMP (a = 1.59; b = 4.0), (D) 2,6-DMP (a = 1.39; b = 4.0), and (E) 2,4,6-TMP (a = 1.05; b= 4.6). In each panel, the red and green arrows indicate the calculated maximum total translational energy release $[E_T^{max}]$ corresponding to CH_3 bond dissociation labeled as "*x*" and "*y*", respectively, in Figure 1. Raw symmetrized velocity map image (top) and the corresponding reconstructed image (bottom) of the methyl group are shown in each case. All of the images are on the same scale, and the double-sided arrow in the first panel shows the direction of the laser polarization. The deviation on the higher energy tail part is due to the multiphoton process and is neglected in the fitting.

The agreement between the calculated $[E_T^{max}]$ value and the experimental observation has been rationalized by fitting the experimental $P(E_T)$ profile to an empirical function of eq 2[44]

$$P(E_T) = C \times ((E_T)^a \times (E_T^{max} - E_T)^b \quad (2)$$

where a and b are adjustable parameters, C is a normalization constant, and E_T^{max} represents the maximum total translational energy available for the fragments in the center-of-mass frame after dissociation. In eq 2, a = 0.5 indicates *a priori* statistical distribution and a > 3 indicates nonstatistical distribution. On

https://doi.org/10.1021/acsomega.3c08705
ACS Omega 2024, 9, 8173−8178

Table 1. Energies (eV) for Various Excitation Processes are Shown in the Energy-Level Schematic (Figure 3)

	BDE(S_0)	BDE(D_0)	$S_0 \rightarrow S_1$	IE	$E_T^{max}(x)$	$E_T^{max}(y)$
2,3-DMP	4.31	2.71	4.61	8.95	2.31	1.76
2,4-DMP	4.32	2.89	4.59	8.89	2.21	1.40
2,5-DMP	4.35	2.59	4.55	9.22	2.16	1.55
2,6-DMP	4.31	2.85	4.6	8.84	2.28	
2,4,6-TMP	4.29	2.84	4.66	8.69	2.45	1.59

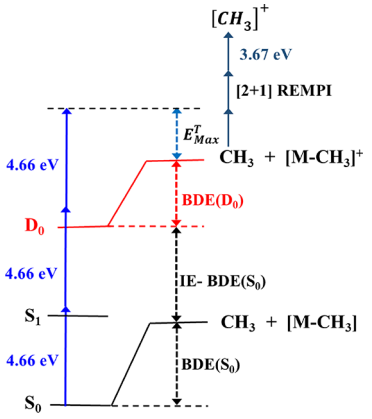

Figure 3. Generalized schematic of the energy-level scheme for the $\{sp^2\}C-C\{sp^3\}$ bond dissociation for DMPs and TMP in various states. The terms used are as follows: S_0: neutral ground state; S_1: first excited state; D_0: cationic ground state; BDE(S_0) and BDE(D_0): $\{sp^2\}C-C\{sp^3\}$ bond dissociation energy in the S_0 and D_0 states, respectively; CH_3: methyl radical; $[M-CH_3]$: co-fragment obtained by loss of one methyl group from parent molecule; IE: ionization energy; E_T^{max}: maximum translational energy available for the fragments in the center-of-mass frame.

the other hand, $0.5 < a < 3$ indicates deviations from *a priori* statistical distribution.[45] Moreover, the value of b indicates the contribution of the rovibrational density of the product states.[44] However, it must be pointed out that the E_T^{max} value also includes the electron kinetic energy after ionization; therefore, E_T^{max} is the sum of kinetic energies of the electron and the mass fragments. The fits to the (E_T) profiles of the methyl radical with eq 2 by fixing the E_T^{max} value corresponding to the dissociation of the methyl group labeled as x (see Table 1) resulted b values in the range of 3.5−4.3 and about 4.7 in the case of dimethylpyridines and trimethylpyridine, respectively. In all the cases, the deviations to fits observed for the higher energy part of $P(E_T)$ is to be attributed to the multiphoton processes and is neglected.[44] Global analysis was carried out by fixing the values of parameter b as 4 and 4.7 for dimethylpyridines and trimethylpyridine, respectively, and reflects the fact that the density of states for trimethylpyridine will indeed be higher as compared to dimethylpyridines due to the presence of an additional methyl group. On the other hand, a comparison of values of a (see the Figure 2 caption and Table S1) suggests that the extent of *a priori* statistical distribution of excess energy is the lowest in the case of 2,4-DMP (a = 1.71) followed by 2,5-DMP (a = 1.59), 2,6-DMP (a = 1.39), and 2,3-DMP (a = 1.11). A relatively better statistical *a priori* distribution in the case of 2,4,6-TMP (a = 1.05) is attributed to a higher density of states. Based on these results, it can be inferred that the dynamics of $\{sp^2\}C-C\{sp^3\}$ bond dissociation in methyl pyridines are marginally dependent on the number and position of the methyl groups. Furthermore, the agreement between the calculated and experimental total translational energy release profiles indicates a clear preference for the dissociation of the $\{sp^2\}C-C\{sp^3\}$ bond closer to the nitrogen atom over the one that is away from the nitrogen in all of the cases.

The remarkable agreement between the calculated $\{sp^2\}C-C\{sp^3\}$ bond dissociation energies and the experimental data indicates that the dissociation of the methylpyridines occurs from the cationic ground state through a [1 + 1 + 1] three-photon dissociation process, which is favored due to the lower dissociation energy in comparison to the neutral ground state. Importantly, the observed dissociation dynamics of the $\{sp^2\}C-C\{sp^3\}$ bond in methylpyridines are similar to methylbenzenes (xylenes)[33] and suggest that the nitrogen atom substitution in the ring has only a marginal effect on the dissociation dynamics of the system. However, a favored dissociation of the $\{sp^2\}C-C\{sp^3\}$ bond adjacent to the nitrogen is observed in the case of methylpyridines, unlike methylbenzenes. The differences in the dissociative ionization of methylbenzenes and methylpyridines can be attributed to the relative stability of the resulting radical cation. In general, the dissociative ionization of the methylbenzenes and methylpyridines leading to the formation of the methyl group is favored due to the lowering of the $\{sp^2\}C-C\{sp^3\}$ bond energy in the cationic ground state relative to the neutral ground state.

CONCLUSIONS

The $\{sp^2\}C-C\{sp^3\}$ bond dissociation channel leading to the formation of the methyl radical for various positional isomers of DMPs and TMP was investigated following 266 nm excitation using a velocity map imaging technique. The ground (ν = 0) state of the methyl radical produced in the dissociation process was detected using a [2 + 1] REMPI scheme using a 333.45 nm laser. The images of the methyl fragment obtained were isotropic, suggesting the longer time scale of the bond dissociation as compared to the rotational reorientation time. The broad total translational energy distribution profiles were obtained in all the cases and were attributed to $\{sp^2\}C-C\{sp^3\}$ bond dissociation in the cationic state following a resonant [1 + 1 + 1] three-photon process due to the lowering of the $\{sp^2\}C-C\{sp^3\}$ bond dissociation energy relative to the neutral ground state. These results were further rationalized based on the fitting of experimental translational energy distribution profiles of the methyl fragment with an empirical function, indicating that the dynamics of $\{sp^2\}C-C\{sp^3\}$ bond dissociation in methyl pyridines is marginally dependent on the number and position of the methyl groups. Interestingly, the results for the $\{sp^2\}C-C\{sp^3\}$ bond dissociation channel upon 266 nm excitation in the case of methylpyridines were found to be similar to those of alkylbenzenes, which suggests that the presence of nitrogen in the ring has only a marginal effect on the dissociation dynamics. However, a preferential dissociation of the $\{sp^2\}C-C\{sp^3\}$ bond ortho to the nitrogen atom over the other $\{sp^2\}C-C\{sp^3\}$ bond is observed due to the inherent asymmetry of the system and is attributed to the relative stability of the resulting radical cation.

ASSOCIATED CONTENT

Supporting Information

The Supporting Information is available free of charge at https://pubs.acs.org/doi/10.1021/acsomega.3c08705.

Mass spectra recorded under various conditions and a table listing the fitting parameters (PDF)

https://doi.org/10.1021/acsomega.3c08705
ACS Omega 2024, 9, 8173−8178

AUTHOR INFORMATION

Corresponding Author

G. Naresh Patwari − *Department of Chemistry, Indian Institute of Technology Bombay, Mumbai 400076, India;* orcid.org/0000-0003-0811-7249; Email: naresh@chem.iitb.ac.in

Authors

Sumitra Singh − *Department of Chemistry, Indian Institute of Technology Bombay, Mumbai 400076, India;* orcid.org/0000-0001-5106-4520

Monali Kawade − *Department of Chemistry, Indian Institute of Technology Bombay, Mumbai 400076, India;* orcid.org/0000-0001-7343-5951

Complete contact information is available at: https://pubs.acs.org/10.1021/acsomega.3c08705

Notes

The authors declare no competing financial interest.

ACKNOWLEDGMENTS

S.S. thanks DST-INSPIRE for the research fellowship. M.K. is supported by the Women Scientists Scheme of the Department of Science and Technology (grant no. SR/WOS-A/CS-18/2019). The authors wish to thank Dr. Namitha Brijit Bejoy for her help with the experiments. Authors gratefully acknowledge the SpaceTime-2 supercomputing facility at IIT Bombay for the computing time. The support and the resources provided by "PARAM Brahma Facility" under the National Supercomputing Mission, Government of India at the Indian Institute of Science Education and Research (IISER) Pune are gratefully acknowledged. This study is based upon a work supported in part by the Science and Engineering Research Board of the Department of Science and Technology (grant no. CRG/2022/005470) and the Board of Research in Nuclear Sciences (BRNS grant no. 58/14/18/2020) to G.N.P.

REFERENCES

(1) Lee, S. A.; White, J. M.; Noyes, W. A. Some Aspects of Benzene Vapor Phase Photochemistry. *J. Chem. Phys.* **1976**, *65*, 2805−2811.

(2) Tseng, C.; Dyakov, Y. A.; Huang, C.; Mebel, A. M.; Lin, S. H.; Lee, Y. T.; Ni, C. Photoisomerization and Photodissociation of Aniline And 4-Methylpyridine. *J. Am. Chem. Soc.* **2004**, *126*, 8760−8768.

(3) Tseng, C.; Lee, Y. T.; Ni, C.; Chang, J. Photodissociation Dynamics of the Chromophores of the Amino Acid Tyrosine: P-Methylphenol, p-Ethylphenol, and p-(2-Aminoethyl) Phenol †. *J. Phys. Chem. A* **2007**, *111*, 6674−6678.

(4) Yokoyama, A.; Zhao, X.; Hintsa, E. J.; Continetti, R. E.; Lee, Y. T. Molecular Beam Studies of the Photodissociation of Benzene at 193 and 248 Nm. *J. Chem. Phys.* **1990**, *92*, 4222−4233.

(5) Afshan, G; Ghorai, S; Rai, S; Pandey, A; Majumder, P.; Patwari, G. N.; Dutta, A Expanding the Horizon of Bio-Inspired Catalyst Design with Tactical Incorporation of Drug Molecules. *Chem. - Eur. J.* **2023**, *29*, No. e202203730.

(6) Lago, A. F.; Januário, R. D.; Simon, M.; Dávalos, J. Z. VUV Photodissociation of Thiazole Molecule Investigated by TOF-MS and Photoelectron Photoion Coincidence Spectroscopy. *J. mass Spectrom.* **2014**, *49*, 1163−1170.

(7) Blank, D. A.; North, S. W.; Lee, Y. T. The Ultraviolet Photodissociation Dynamics of Pyrrole. *J. Chem. Phys.* **1994**, *187*, 35−47.

(8) Lin, M. F.; Dyakov, Y. A.; Tseng, C. M.; Mebel, A. M.; Hsien Lin, S.; Lee, Y. T.; Ni, C. K. Photodissociation Dynamics of Pyridine. *J. Chem. Phys.* **2005**, *123*, No. 054309.

(9) Lin, M. F.; Dyakov, Y. A.; Tseng, C. M.; Mebel, A. M.; Hsien Lin, S.; Lee, Y. T.; Ni, C. K. Photodissociation Dynamics of Pyrimidine. *J. Chem. Phys.* **2005**, *123*, No. 084303.

(10) Sengupta, S.; Kumar, A.; Naik, P. D.; Bajaj, P. The Dynamics of OH Generation by Photodissociation of Morpholine Molecule at 193 Nm. *Chem. Phys. Lett.* **2008**, *465*, 197−202.

(11) Chachisvilis, M.; Zewail, A. H. Femtosecond Dynamics of Pyridine in the Condensed Phase: Valence Isomerization by Conical Intersections. *J. Phys. Chem. A* **1999**, *103* (37), 7408−7418.

(12) Tsai, S. T.; Lin, C. K.; Lee, Y. T.; Ni, C. K. Dissociation Rate of Hot Benzene. *J. Chem. Phys.* **2000**, *70*, 67−70.

(13) Ni, C.; Tseng, C.; Lin, M.; Dyakov, Y. A. Photodissociation Dynamics of Small Aromatic Molecules Studied by Multimass Ion. *J. Phys. Chem. B* **2007**, *111*, 12631−12642.

(14) Wilzbach, K. E.; Harkness, A. L.; Kaplan, L. The Photochemical Rearrangement of Benzene-1, 3, 5-D3. *J. Am. Chem. Soc.* **1968**, *90*, 1116−1117.

(15) Burgstahler, A. W.; Chien, P. Photochemical Isomerization of Di-Z-Butylbenzenes. *J. Am. Chem. Soc.* **1964**, *86*, 2940.

(16) Kaplan, L.; Wilzbach, K. E.; Brown, W. G.; Yang, S. S. Phototransposition of Carbon Atoms in the Benzene Ring. *J. Am. Chem. Soc.* **1965**, *87*, 675−676.

(17) Pavlik, J. W.; Kebede, N.; Thompson, M.; Day, A. C.; Barltrop, J. A. Vapor-Phase Photochemistry of Dimethylpyridines. *J. Am. Chem. Soc.* **1999**, *121*, 5666−5673.

(18) Pavlik, J. W.; Laohhasurayotin, S.; Vongnakorn, T. Vapor-Phase Photochemistry of Methyl- and Cyanopyridines: Deuterium Labeling Studies. *J. Org. Chem.* **2007**, *73*, 7116−7124.

(19) Cao, J.; Fang, Q.; Fang, W. H. Photoisomerization Mechanism of 4-Methylpyridine Explored by Electronic Structure Calculations and Nonadiabatic Dynamics Simulations. *J. Chem. Phys.* **2011**, *134*, No. 0443071.

(20) Brand, U.; Hippler, H.; Lindemann, L.; Troe, J. C-C and C-H Bond Splits of Laser-Excited Aromatic Molecules. 1. Specific and Thermally Averaged Rate Constants. *J. Phys. Chem.* **1990**, *94*, 6305−6316.

(21) Park, J.; Bersohn, R.; Oref, I. Unimolecular Decomposition of Methylsubstituted Benzenes into Benzyl Radicals and Hydrogen Atoms. *J. Chem. Phys.* **1990**, *93*, 5700−5708.

(22) Nakashima, N.; Yoshihara, K. Role of Hot Molecules Formed by Internal Conversion in UV Single-Photon And. *J. Phys. Chem.* **1989**, *93*, 7763−7771.

(23) Luther, K.; Troe, J.; Weitzel, K. C-C and C-H Bond Splits of Laser-Excited Aromatic Molecules. 2. In Situ Measurements of Branching Ratios. *J. Phys. Chem.* **1990**, *94*, 6316−6320.

(24) Hippler, H.; Schubert, V.; Troe, J.; Wendelken, H. J. Direct Observation of Unimolecular Bond Fission in Toluene. *Chem. Phys. Lett.* **1981**, *84*, 253−256.

(25) Huang, C. L.; Jiang, J. C.; Lee, Y. T.; Ni, C. K. Photoisomerization and Photodissociation of Toluene in Molecular Beam. *J. Phys. Chem. A* **2003**, *107*, 4019−4024.

(26) Huang, C. L.; Jiang, J. C.; Lee, Y. T.; Ni, C. K. Photoisomerization and Photodissociation of m -Xylene in a Molecular Beam. *J. Phys. Chem. A* **2003**, *107*, 4019−4024.

(27) Pavlik, J. W.; Kebede, N.; Opatz, T. Phototransposition Chemistry of Pyridine and Substituted Pyridines in the Vapor Phase. *Arkivoc* **2018**, 1−18.

(28) Held, A.; Selzle, H. L.; Schlag, E. W. Methyl Group Rotational Dynamics in O-, m-, and p-Xylene Cations from Pulsed Field Ionization Zero-Kinetic-Energy Spectroscopy. *J. Phys. Chem. A* **1998**, *102*, 9625−9630.

(29) Mcmillen, D. F.; Golden, D. M. Hydrocarbon Bond Dissociation Energies. *Annu. Rev. Phys. Chem.* **1982**, *33*, 493−532.

(30) Chen, C. H.; Mccann, M. P. Measurements of Two - Photon Absorption Cross Sections for Liquid Benzene and Methyl Benzenes. *J. Chem. Phys.* **1988**, *88*, 4671−4677.

(31) Scott, T. W.; Braun, C. L.; Albrecht, A. C. Multiphoton Ionization in the Organic Condensed Phase: A Three - Photon Study of Liquid Benzene. *J. Chem. Phys.* **1982**, *76*, 5195−5202.

(32) Zhou, Z.; Xie, M.; Wang, Z.; Qi, F. Determination of Absolute Photoionization Cross-Sections of Aromatics and Aromatic Derivatives. *Rapid Commun. Mass Spectrom.* **2009**, *23*, 3994−4002.
(33) Bejoy, N. B.; Kawade, M.; Singh, S.; Patwari, G. N. Dynamics of Methyl Radical Formation Following 266 Nm Dissociative Photoionization of Xylenes and Mesitylene. *J. Phys. Chem. A* **2022**, *126*, 1960−1965.
(34) Mishra, S.; Bejoy, N. B.; Kawade, M.; Upadhyaya, H. P.; Patwari, G. N. Photodissociation of O-Xylene at 266 Nm: Imaging the CH3 Dissociation Channel. *J. Chem. Sci.* **2021**, *133*, 128.
(35) Li, W.; Chambreau, S. D.; Lahankar, S. A.; Suits, A. G. Megapixel Ion Imaging with Standard Video. *Rev. Sci. Instrum.* **2005**, *76*, No. 063106.
(36) Schneider, C. A.; Rasband, W. S.; Eliceiri, K. W. NIH Image to ImageJ: 25 Years of Image Analysis. *Nat. Methods* **2012**, *9*, 671−675.
(37) Dribinski, V.; Ossadtchi, A.; Mandelshtam, V. A.; Reisler, H. Reconstruction of Abel-Transformable Images: The Gaussian Basis-Set Expansion Abel Transform Method. *Rev. Sci. Instrum.* **2002**, *73*, 2634.
(38) Hudgens, J. W.; DiGiuseppe, T. G.; Lin, M. C. Two Photon Resonance Enhanced Multiphoton Ionization Spectroscopy and State Assignments of the Methyl Radical. *J. Chem. Phys.* **1983**, *79*, 571−582.
(39) Chandler, D. W.; Thoman, J. W.; Janssen, M. H. M.; Parker, D. H. Photofragment Imaging: The 266 Nm Photodissociation of CH3I. *Chem. Phys. Lett.* **1989**, *156*, 151−158.
(40) Vinklárek, I. S.; Rakovský, J.; Poterya, V.; Fárník, M. Clustering and Multiphoton Effects in Velocity Map Imaging of Methyl Chloride. *Mol. Phys.* **2021**, *119*, No. e1823507.
(41) Bain, M.; Hansen, C. S.; Ashfold, M. N. R. Communication: Multi-Mass Velocity Map Imaging Study of the Ultraviolet Photodissociation of Dimethyl Sulfide Using Single Photon Ionization and a PImMS2 Sensor. *J. Chem. Phys.* **2018**, *149*, No. 081103.
(42) Baboul, A. G.; Curtiss, L. A.; Redfern, P. C.; Raghavachari, K. Gaussian-3 Theory Using Density Functional Geometries and Zero-Point Energies. *J. Chem. Phys.* **1999**, *110*, 7650−7657.
(43) Frisch, M. J.; Trucks, G. W.; Schlegel, H. B.; Scuseria, G. E.; Robb, M. A.; Cheeseman, J. R.; Scalmani, G.; Barone, V.; Mennucci, B.; Petersson, G. A.; et al. *Gaussian 09, Revision D.01*; Gaussian Inc.: Wallingford, CT, 2009.
(44) Matthaei, C. T.; Mukhopadhyay, D. P.; Fischer, I. Photodissociation of Benzoyl Chloride: A Velocity Map Imaging Study Using VUV Detection of Chlorine Atoms. *J. Phys. Chem. A* **2021**, *125*, 2816−2825.
(45) Quack, M. Statistical Models for Product Energy Distributions in Bimolecular Reactions with Metastable Intermediates. *Chem. Phys.* **1980**, *51*, 353−367.

https://doi.org/10.1021/acsomega.3c08705
ACS Omega 2024, 9, 8173−8178